

Effective Light Directed Assembly of Building Blocks with Microscale Control

Ngoc-Duy Dinh, Rongcong Luo, Maria Tankeh Asuncion Christine, Weikang Nicholas Lin, Wei-Chuan Shih, James Cho-Hong Goh, and Chia-Hung Chen*

Light-directed forces have been widely used to pattern micro/nanoscale objects with precise control, forming functional assemblies. However, a substantial laser intensity is required to generate sufficient optical gradient forces to move a small object in a certain direction, causing limited throughput for applications. A high-throughput light-directed assembly is demonstrated as a printing technology by introducing gold nanorods to induce thermal convection flows that move microparticles (diameter = 40 μm to several hundreds of micrometers) to specific light-guided locations, forming desired patterns. With the advantage of effective light-directed assembly, the microfluidic-fabricated monodispersed biocompatible microparticles are used as building blocks to construct a structured assembly (≈ 10 cm scale) in ≈ 2 min. The control with microscale precision is approached by changing the size of the laser light spot. After crosslinking assembly of building blocks, a novel soft material with wanted pattern is approached. To demonstrate its application, the mesenchymal stem-cell-seeded hydrogel microparticles are prepared as functional building blocks to construct scaffold-free tissues with desired structures. This light-directed fabrication method can be applied to integrate different building units, enabling the bottom-up formation of materials with precise control over their internal structure for bioprinting, tissue engineering, and advanced manufacturing.

1. Introduction

The conventional tissue engineering top-down approach to manufacturing, in which a mold is first prepared for object uploading, followed by molecular curing,^[1] has been widely

used to prepare structured constructs, but the challenges associated with precise control over the microenvironment remain to be resolved. For example, scaffolds fabricated for cell uploading in tissue engineering are subject to the limitations of low-density cell growth and slow/uneven

N.-D. Dinh, Dr. R. Luo, M. T. A. Christine, W. N. Lin,
Prof. J. C.-H. Goh, Dr. C.-H. Chen
Department of Biomedical Engineering
National University of Singapore
21 Lower Kent Ridge Road, Singapore 119077
E-mail: biecch@nus.edu.sg

Prof. W.-C. Shih
Departments of Electrical
and Computer Engineering
Biomedical Engineering and Chemistry
University of Houston
4800 Calhoun Rd, Houston, TX 77004, USA

DOI: 10.1002/sml.201700684

Prof. J. C.-H. Goh
Department of Orthopaedic Surgery
Yong Loo Lin School of Medicine
National University of Singapore
21 Lower Kent Ridge Road, Singapore 119077
Dr. C.-H. Chen
Singapore Institute of Neurotechnology (SINAPSE)
National University of Singapore
21 Lower Kent Ridge Road, Singapore 119077
Dr. C.-H. Chen
Biomedical Institute for Global Health Research & Technology
(BIGHEART)
National University of Singapore
21 Lower Kent Ridge Road, Singapore 119077



medium diffusion in the bulk.^[2] Recently, the use of bottom-up assembly to integrate various nano/microscale building blocks has attracted increasing attention for the advanced manufacturing of functional units as a natural tissue hierarchy, showing promise in applications such as electronic components,^[3] photonic crystals,^[4] and 3D cell assembly.^[5] However, most bottom-up approaches rely on patterning technologies, such as acoustics,^[6] magnetic^[7] or liquid templates,^[8] and enzymes,^[9] and thus lack arbitrary structural control at the microscale. To improve the microscale control of such bottom-up approaches, a series of advanced fabrication technologies have been investigated, including microfluidic guidance,^[10] surface tension,^[11] DNA targeting,^[12] magnetics,^[13] robotics,^[14] electrowetting.^[15] However, these methods exist limitations such as assembly fewer number of building blocks, low throughput and costly. Beside the building blocks assembling strategy, a comprehensive bottom-up approach 3D bioprinting^[16,17] in which the materials are directly printed and formed desirable structures after polymerization was recently proposed. However, these technologies are subject to limitations in the restricted flexibility of materials selection, biocompatibility, and high-level structure.

Light-directed technologies, such as optical tweezers,^[18] optoelectronics tweezers,^[19] and fiber devices,^[20] offer precise control of the movement of nano/microscale objects to manipulate functional units. However, the optical forces are insufficient to move large objects ($\approx 100\ \mu\text{m}$ in diameter), such as microtissue assemblies, hydrogel particles, and tissue building blocks, and the throughput of the assembly method is limited ($\approx 5\text{--}10\ \mu\text{m}$ laser spot diameter). In fact, high laser intensities are usually required to generate sufficient optical forces to pattern the objects, which might damage micro-bio-objects, such as tissues, and limit biofabrication and throughput for industrial applications.

To enhance optical forces, researchers developed arrays of plasmonic nanoantennas^[21] to convert light energy into local heat-generating convection flows for object assembly. With the integration of plasmonic nanostructures and electrokinetics,^[22] significant electrothermal convection was generated, enabling programmable object trapping and patterning through variations in laser intensity. Nevertheless, with plasmonic methods, arbitrary control over the configuration was not easily achieved because the assembled structures were predetermined by the patterned nanoarray. Indeed, most of the current bottom-up methods have reached a trade-off between high-throughput assembly and precise arbitrary control of fabrication. To date, a lack of light-directed manipulation technologies exists for the microscale, especially for bottom-up biofabrication using low-power lasers to effectively assemble micro-bio-objects with precise control.

In this study, a novel high throughput light-directed assembly method on the microscale was investigated by suspending gold nanorods (GNRs), as photothermal transducers, in a fluidic medium to induce thermoplasmonic convections for the assembly of building blocks fabricated through microfluidics. Because significant local thermoplasmonic convections were generated by precisely controlling the low-power infrared laser spot size and direction, effective building block assembly with high resolution enabled

the desired patterns. By using an automatic motorized stage with optical source integration, the assemblies with desirable patterns were approached with programmable manner. This method was used as an advanced printing technology to form centimeter-scale functional units in ≈ 10 min by integrating various hydrogel building blocks, which were fabricated using droplet-based microfluidics. It is worth to note that because this light-directed assembly process was independent of the fabrication of the building blocks, a wide range of functional biocompatible materials could be selected to fabricate the building blocks that form the desired structures without the limitations of polymerization during construction inherent to printing.

To illustrate the application of light-directed assembly in bottom-up tissue engineering, we demonstrated that tissue patterns with high cell viability and proliferation after long-term culture can be assembled and printed using mesenchymal stem cell (MSC)-seeded microgel and microtissue (spheroids) as building blocks to form bioinspired microtissues containing an extracellular matrix (ECM) surrounded by MSCs. Excellent cell viability and proliferation were characterized in these microtissues after the long-term culturing of the MSC seeded inside. Notably, the low-power near-infrared (NIR) laser used to assemble these building blocks caused only limited stimulations to the MSC during the light-directed process, potentially allowing for building block assembly *in vivo* for direct tissue reconstruction. The presented high-throughput, bottom-up method of building block assembly through precise thermoplasmonic convective flow controls can revolutionize current biofabrication processes that otherwise would have been difficult to achieve using 3D printing and other assembly technologies.

2. Results and Discussion

2.1. The Concept of Light-Directed Assembly Using the Gold Nanorod Suspension

GNRs with an absorption wavelength of 800 nm were suspended in an aqueous medium together with the objects to be assembled (e.g., microtissue, spheroids, cell seeded-hydrogel microparticles, or cell-laden microgels). Under NIR laser irradiation (wavelength 808 nm, matched with the absorbance frequency of the GNRs), a localized surface plasmon resonance was triggered. Most of the electrons on the GNR surface oscillated to produce substantial electric fields in the immediate vicinity of the GNRs.^[23] Accordingly, GNRs were used to convert light into local heating, immediately causing the local heat to induce convection flow, or so-called thermoplasmonic convection. This convection generated the flow to carry suspended objects to the center of the light spot (**Figure 1a**; Video S1, Supporting Information) under irradiation by a low-power NIR laser. In a control experiment, hydrogel building blocks without GNRs did not move in the solution under irradiation (Video S2, Supporting Information). To make the building blocks monodispersed and biocompatible, we fabricated hydrogel particles (polyethylene (glycol) diacrylate (PEGDA) and gelatin methacryloyl

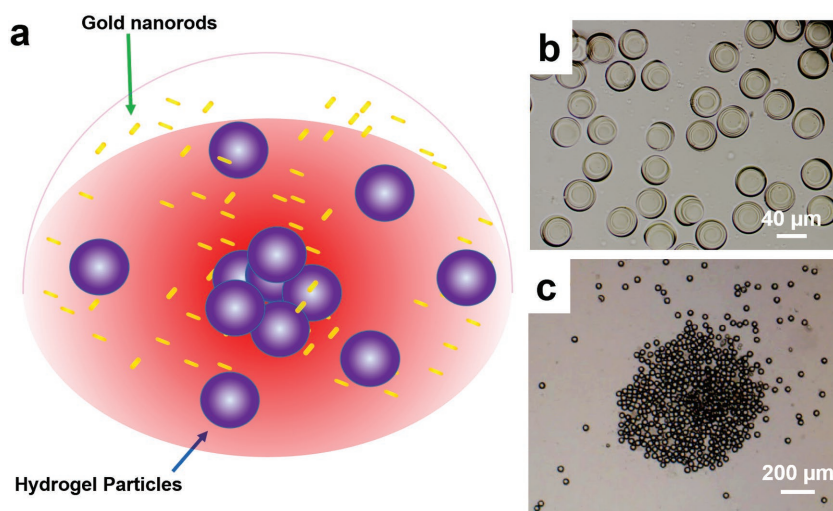


Figure 1. Principle of light assembly of microparticles through plasmonic nanoparticles (gold nanorods (GNRs)). a) An illustration of microparticle aggregates resulting from GNRs moving to the center of the light spot, and the GNRs absorbing light to convert to heat, which induced thermal convection. b) The random distribution of hydrogel (PEGDA + GelMA) microparticles in water. The hydrogel particles were synthesized through microfluidic encapsulation. c) The hydrogel particle assembly in the center of the laser spot.

(GelMA) diameter = 40 μm) using droplet-based microfluidics (Figure 1b; Figure S1, Supporting Information). With thermal-enhanced convection, a high throughput assembly of these building blocks was achieved at the large laser spot, where thousands of building blocks aggregated to the center of the laser spot (Figure 1c).

2.2. Simulation and Characterization of GNRs

GNRs were synthesized via an established method^[24] and were subsequently characterized by transmission electron microscopy (TEM) (Figure 2a) and zeta-potential measurements (31.98 ± 1.06 mV). Their size was measured by dynamic light scattering (40.23 ± 2.19 nm). The COMSOL and Lumerical software packages were used to simulate the thermal-enhanced convection flows by solving the differential equations for electromagnetic, heat transfer, and fluid mechanics. When the GNRs interacted with the stimulation light, the electric field pushed the free electrons on the GNR surface to one side. As a result, the electrons' negative charges accumulated on one side, and the positive charges remained on another side. The negatively charged side of a GNR reacted with the positively charged side of another GNR, causing electron oscillations. When the frequency of incident light coincided with the natural oscillation frequency of the GNRs, large oscillations of free electrons occurred on the GNRs. Thus, a strong electric field called a localized surface plasmon resonance was produced around the GNRs. The simulated electric field generated by solving the time-independent vector wave equation is shown in Figure 2b. When the GNRs accumulated at the center of the laser spot, the coupling between plasmon resonances was triggered. As a result, the local fields were substantially enhanced (Figure 2c) and produced heat, causing the local temperature to increase

in the vicinity of the GNRs (Figure 2d). The plasmonic heating was solved by the finite-difference time-domain method (Section S1, Supporting Information). The local temperature increase was dependent on the laser power, GNR concentration, and time period (Figure S2, Table S1, Supporting Information). The local temperature increase induced convection flow, which is called thermoplasmonic convection. COMSOL software was used to analyze the convection profile (Figure 2e).

In our experiments, the temperature increased by 32 $^{\circ}\text{C}$ from room temperature (26 $^{\circ}\text{C}$) after 60 s when a 0.6 W cm^{-2} NIR laser was used; by contrast, in the absence of the GNRs, the temperature increased by 4 $^{\circ}\text{C}$ (Figure 2f,g). A Gaussian beam was used in our simulation. The GNR sizes correspond to their absorbance wavelengths. Three GNR wavelengths (650, 800, and 915 nm) were measured. The 800 nm GNRs, whose length matched the laser wavelength, were used in our experiments.

The GNRs were coated with bovine serum albumin (BSA) to reduce the toxicity of the GNRs (Figure S3, Supporting Information).

It is worth to note that under the laser irradiation thermoplasmonic convection was generated to flow the microscaled hydrogel particles to the centre of laser spot. Because of the heavy mass of microscale hydrogel particle, the vertical microflow convection generated was not sufficient to flow these microscale hydrogel particles away from the centre. Therefore, the microscaled hydrogel particles were remained in the centre of laser spot. However, suspended nanosized GNRs were flowed through vertical microflow convection to be away from the laser spot centre according to the flow pattern of generated microconvection.

2.3. Spatial and Temporal Control of Hydrogel Microparticle Assembly

The laser spot was adjusted to ≈ 10 μm (determined by the objective lens of a microscope), which was similar to the optical tweezers' size and was suitable to control single particles (diameter, 40 μm). Hydrogel particles fabricated by microfluidics were driven to the center of the laser beam and the highest light intensity (Figure 3a). The trapping force was dependent on the GNR concentration and the laser intensity (Figure 3b) and was calculated using the so-called hydrodynamic-drag method.^[25] To demonstrate precise control of light-directed assembly, individual hydrogel particles were assembled in lines two, three, four, or five units long (Figure 3c). Notably, the direct optical trapping method required a high-intensity pulse laser (≈ 500 kW cm^{-2}) to trap a single large PEGDA particle (diameter 80 μm).^[26] Using the light-directed method, we manipulated large hydrogel particles (diameter ≈ 300 μm) using a low-power laser (< 1 W cm^{-2}) for

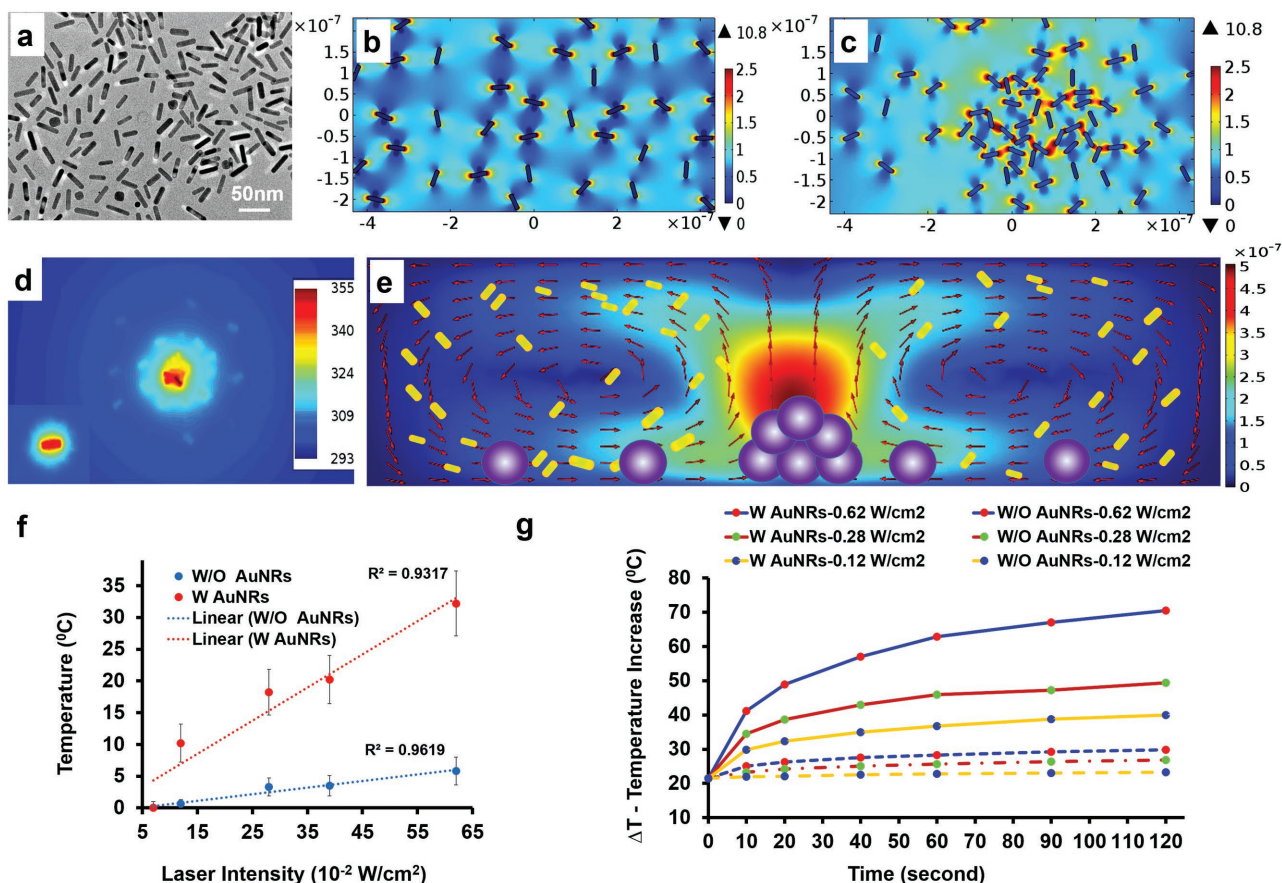


Figure 2. Gold nanorod (GNR) synthesis, simulation, and characterization. a) TEM image of the GNRs (40×10 nm). b) The electric fields (V m^{-1}) of the GNRs in a random distribution. c) The E-fields of the GNRs showed significant enhancement upon aggregation. d) The temperature increased due to near-infrared laser illumination, unit (K). e) Illustration of the convection profile due to local temperature increases from the absorption by the GNRs of energy from light and conversion into heat (m s^{-1}). This flow carried hydrogel microparticles to the center of the laser spot. f) The correlation between the temperature increase and laser intensity in the absence and presence of GNRs (concentration 1×10^{-6} M). g) The correlations among the temperature increase, laser intensity, and time (1.4×10^{-6} M GNR).

effective assembly in bioapplications, particularly favoring tissue engineering. In addition, the precise control of the assembly of different hydrogel particles indicated by yellow/green colors was demonstrated (Figure 3d), showing the potential for applications in the construction of functional biological units by a variety of cells and tissues in a programmable manner.

2.4. High-Throughput Assembly of Building Blocks

To perform high-throughput assembly with programmable control, an automatic stage integrated with an NIR light source (FC-808-2W, Optoelectronics Tech. Co., Ltd) was developed. The laser was installed on a customized XYZ motorized stages. The distance between the light source and hydrogel building blocks was 6 mm to ensure the laser spot size was optimized around 1 mm in diameter. The laser intensity was set at 0.38 W/cm^2 . With this experimental setting the force applied to each building blocks was characterized to be $\approx 50 \text{ pN}$ to move the particles toward to the center of the light spot. The assembly of ≈ 1000 hydrogel particles was approached by controlling the motorized stage for assembly

within ≈ 2 min (Figure 4a). The hydrogel particles were directed to the center of the laser spot, forming an aggregation 1 mm in diameter within 30 s (Figure 4b). Three different sizes of particles (40, 80, and $236 \mu\text{m}$) were used in our experiments. The correlation between the number of different particles aggregated and the time period was calibrated (Figure 4c). Moreover, increases in laser power corresponding to velocity, trapping force, and GNR absorbance wavelength are calculated (Figure 4d) using the hydrodynamic-drag method.^[25] The GNRs absorbed the maximum laser energy when the absorbance frequency matched the incident light frequency, resulting in surface resonance, which in turn caused a local temperature increase. For example, although 650 nm GNRs and 915 nm GNRs absorbed the NIR light (808 nm in wavelength), resulting in a slight increase in temperature, plasmon resonance was not triggered and thus did not contribute to the temperature increase. The plasmon resonance of the 808 nm GNRs was triggered by the NIR light (808 nm in wavelength) to generate substantial heat energy to increase the solution temperature, causing convection flows around the light spot area. The particles moved according to the convection flows. The velocity profiles of the particles are characterized in Figure S4 (Supporting Information).

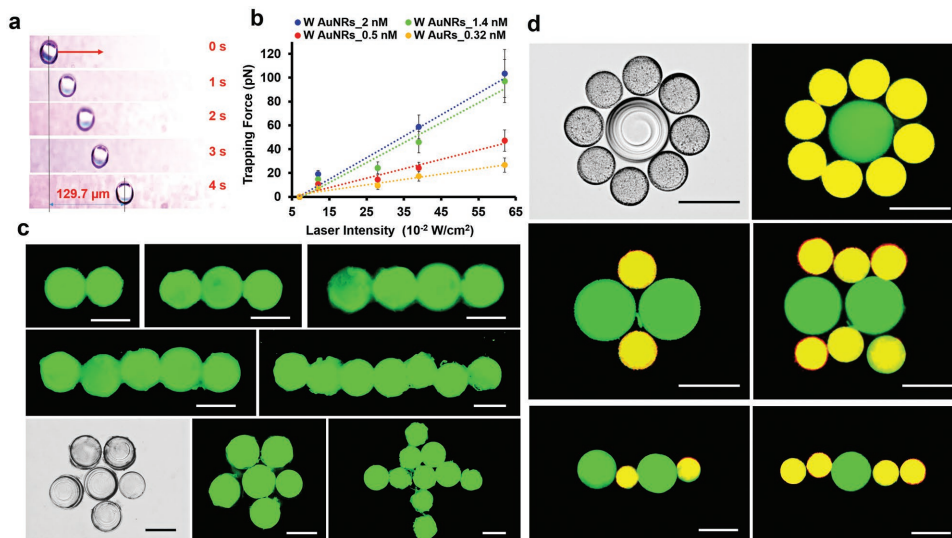


Figure 3. Spatial and temporal control of individual hydrogel microparticles. a) Illustration of single microparticles moving to the center of the light spot. b) The trapping forces increased with increasing laser power and increasing GNR concentration. The forces were estimated on the basis of the method described in a previous report. c) The hydrogel microparticles were assembled into particular shapes such as lines and circles. d) Different hydrogel particles (green and yellow) were controlled to assemble particular shapes. Scale bar: 100 μm .

The patterns and structures of the assembly were programmed through computer and operated by xyz stage and printing systems. For example, the laser spot was moved along certain directions to form an assembly of desired patterns, such as a one-line pattern (Figure 5a–c) and three-line

pattern (Figure 5d,e). A large pattern (2 mm wide \times 10 mm long) was constructed by a large number of 40 μm (PEGDA, GelMA) hydrogel building blocks within 5 min. The building blocks were bonded by crosslinking reagents (fibrinogen and thrombin) (Figure 5f) to form bottom-up 3D-structured

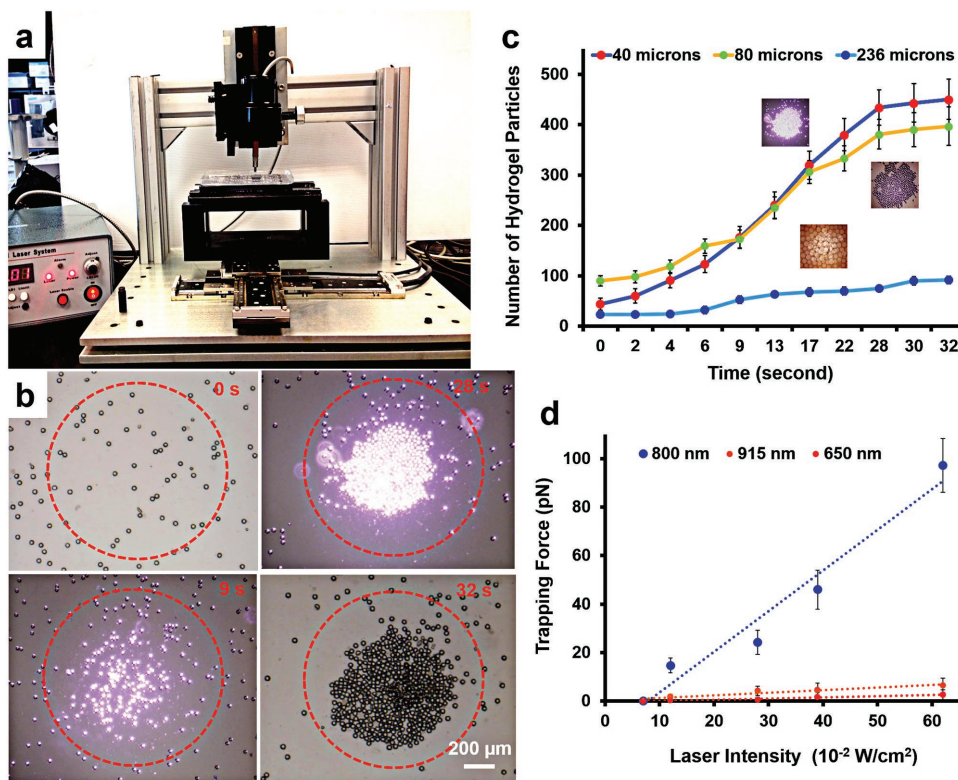


Figure 4. High-throughput light assembly of microparticles by controlling the laser equipped in an automatic stage. a) A customized motorized stage for 3D movement is developed to form the pattern with programmable manner. b) Illustration of microparticle aggregation with a series of still images. c) The number of hydrogel (PEGDA) microparticles assembled in a circle for three sizes of hydrogel particles (40, 80, and 236 μm) as a function of time. d) The trapping force for three GNR wavelengths (650, 800, and 915 nm) with changes in laser intensity.

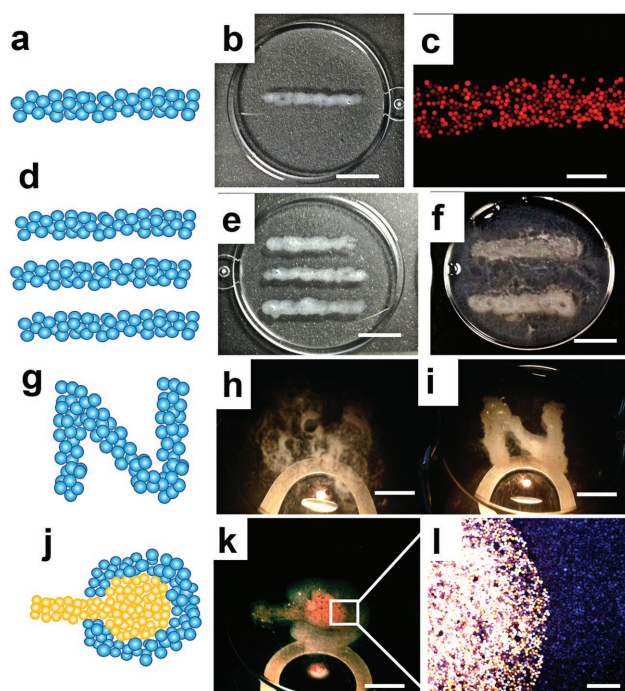


Figure 5. High-throughput light assembly. Illustrations of microparticle aggregates into a–c) a one-line pattern, d,e) three lines, f) the pictures show two lines of microparticles crosslinked by uploading fibrinogen hydrogel, g) special patterns h) before assembly and i) after assembly. A demonstration of two different hydrogel particle assemblies forming patterns as directed by light. j–l) A clock-key shape. Scale bars: (b,e,f,h,i,k) 6 mm, (d) 200 μm , (l) 400 μm .

materials, such as photonic crystals, scaffolds, and 3D tissues. Furthermore, high-level structures (Figure 5g) were constructed using this method before assembly (Figure 5h), after assembly (Figure 5i). To construct a functional assembly formed by different units, we assembled the first-type units into a pattern. We then integrated the second-type units into the first pattern, forming a structure with two different units. This process was repeated to create make a functional structure with high-level hierarchy, such as human tissue. For example, clock-key (Figure 5j–l) was constructed from two different types of hydrogel units, one lighter in color and one blue in color, as demonstrations, revealing complicated and tunable macroscale configurations.

2.5. Light-Directed Assembly of 3D Microtissue

To demonstrate applications in tissue engineering, we used this method to fabricate a 3D microtissue assembly (Figure 6a). The hydrogel particles (building blocks) were sterilized in an autoclave. MSCs were then incubated in a chamber with the hydrogel particles for cell adhesion to the particles. The bright-field images of the single cell-seeded hydrogel particle and pattern were obtained using an inverted microscope (Nikon TE 2000 U) (Figure 6b,c). To enhance the cell adhesion to the hydrogel particles, a glass chamber, onto which cells tended not to attach, was used for seeding cells and particles. After culturing for one to two weeks, the cell-seeded hydrogel particles became sticky for use as the assembly building blocks.

To ensure the biocompatibility of this assembly, we evaluated its cytocompatibility. The cell live/dead assay was performed to characterize cell viability (Figure 6d; Figure S5, Supporting Information). A green color (fluorescein diacetate) indicated living cells, whereas a red color (propidium iodide) indicated dead cells. The cell viability under different laser powers and exposure times was tested (Figure 6e). Under an irradiation laser power of $\approx 0.6 \text{ W cm}^{-2}$ for 30 s, high cell viability ($\approx 80\%$) was observed. After assembly, the cells were incubated for two to three weeks. The cells proliferated and contacted each other to fill the gaps between the particles, forming a bottom-up 3D microtissue with an internal structure based on the pattern of the assembly. To characterize the cell proliferation after assembly, we conducted Alamar Blue assays to illustrate no significant difference between the preassembled cells and the control group (Figure 6f). As expected, under high-power laser radiation, cell proliferation slowed compared to the cell proliferation under low-power laser radiation.

To investigate cell attachment and cell fate in a hydrogel particle, immunocytochemistry was performed by staining the actin with Texas Red-X phalloidin, and the nuclei of cells with Hoechst. The cell-seeded hydrogel particles were observed using an LSM-800 confocal microscope (Figure 7a,b) to show cell attachment and fate in 3D. The cross-sections of the cell-seeded hydrogel particles are reported as well. This 3D image was labeled with the depth to visualize the cellular 3D structure (Figure 7c). As illustrated using the Zen (black edition) program, the cells on top of the hydrogel particles showed a red color, and the cells at the bottom of the particles showed a blue color. Immunocytochemistry was also performed to confirm the cell fate in the assembled scaffold. The cross-section of the 3D image of the free scaffold was observed using an LSM-800 confocal microscope (Figure 7d).

We observed the 3D image of the free scaffold using Zen (black edition) (Figure 7e) to show cell fate and scaffold formation. The scaffold internal structure, such as the pore size and shape, could be controlled via the unit size and assembly process (laser intensity, direction, and irradiation time). Here, the height of the scaffold was 400–500 μm . To visualize the structural details, 3D images of the cell-seeded hydrogel particles and the assembled scaffold were labeled with the depth (Figure 7f). Cell-seeded hydrogel particles in different positions and layers of the assembly are shown in the image. The particles in the top layer exhibited a red color, whereas the particles in the middle/bottom layer exhibited a green/blue color. A movie demonstrating this assembled scaffold from different angles was recorded to provide a 3D view of its structure (Video S3, Supporting Information).

Previously, 3D printing technology has been demonstrated for 3D tissue construction on the microscale.^[16] However, this technology required the selection of specific biopolymers (bioinks such as alginate, gelatin, and PEGDA) and the polymerization of these polymers during cell printing, which affected the cells' activities and proliferation. In fact, for some sensitive cells, such as MSCs, this harsh printing process might trigger the cells to form undesirable products. Several cell/building block methods have been used to form 3D tissues. The building blocks were fabricated

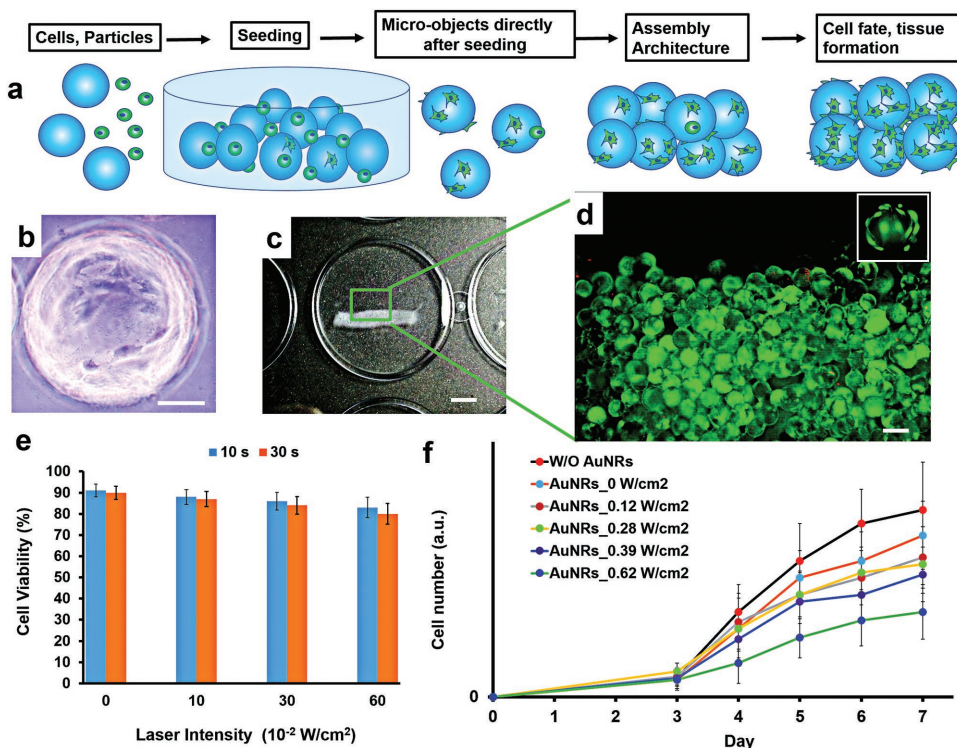


Figure 6. Hydrogel microparticle cell-laden assembly. a) The procedure for the hydrogel microparticle cell-laden assembly. MSCs and particles were seeded into wells for cell adhesion before assembly. Cell-laden hydrogel particles were then assembled into the patterns, the cells met, and the tissue formed. b) A bright-field image of a single cell-seeded microparticle. c) A bright-field image of the cell-seeded microparticles assembly. d) Cell viability after assembly. e) Cell viability for different laser intensities via 10 and 30 s laser exposures. f) Cell proliferation was observed to correlate with laser power and time (day). Scale bars: (b) 50 μ m, (c) 4 mm, and (d) 100 μ m.

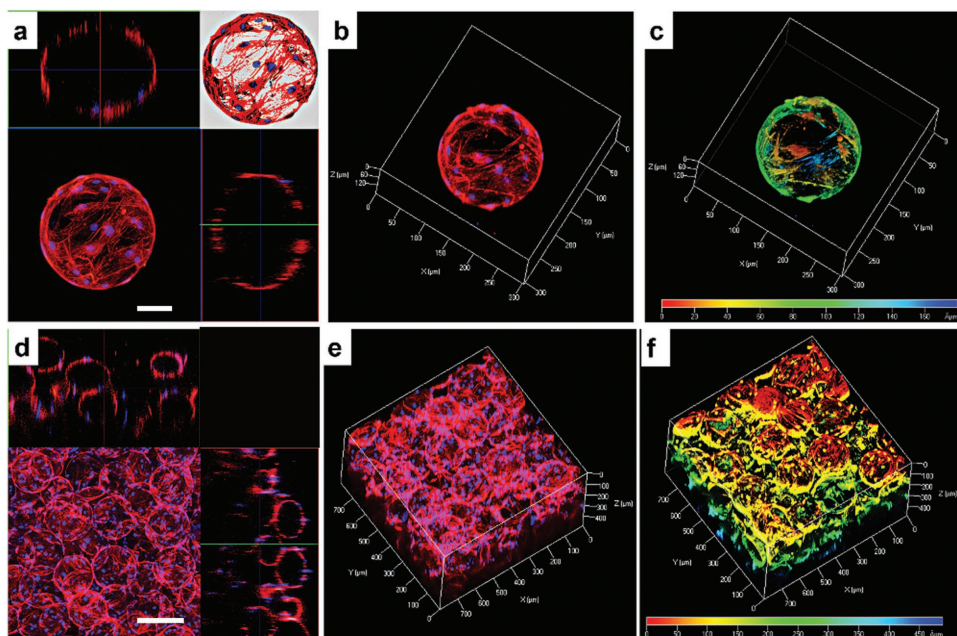


Figure 7. Confocal images. a) Individual cell-seeded hydrogel particles with cross-sections; the actin (red) shows the cell skeleton, and the blue is the cell nucleus. The figure in the corner was plotted with a white background to enhance the view. b) A 3D image of a cell-seeded hydrogel particle. c) The deep coding of a cell-laden hydrogel particle. The red color represents the cells on the top of the particle (0 μ m), whereas the blue color indicates the deepest cells. d) An illustration of the cell scaffold free of the cell-seeded microparticle assembly after 10 d, with the cross-sectional images. e) 3D image of the scaffold of the cell-seeded microparticle assembly. f) The depth coding of the free scaffold. The red color represents the top layer of the cell-seeded microparticles, whereas the blue color indicates the bottom layer of the scaffold. Scale bars: (a) 30 μ m, (d) 120 μ m.

using arbitrary chemical methods without constraints in cell biology and printing procedures. These bottom-up assembly methods separated the building block fabrication step, cell seeding step and the assembly step to enable construction of the desired 3D tissue using flexible optimized biomaterials as a natural tissue with hierarchy.^[27] However, most of these assembly methods exhibit a trade-off between precise arbitrary control and high-throughput manipulation. For example, optical tweezers were used to make 3D tissue with precise microenvironmental control; however, the throughput was only a few cells per minute. Acoustic technology offered a high-throughput assembly of cells according to an acoustic field pattern, although its ability to form arbitrary 3D assembly functional units was limited. Using the technology developed in the present work, we can precisely control the high throughput assembly of cell-seeded hydrogel particles to form a 3D microtissue. In the first step of this process, to fabricate the spheroids, cells were seeded in a microwell array prepared from agarose gel. After 1–2 d of incubation, the MSCs were transformed into spheroids, as evident in Figure S6, Supporting Information. Here, the MSCs were stained with fluorescein diacetate (FDA) to show a green color, whereas the nuclei were dyed with DAPI (4',6-Diamidino-2-Phenylindole, Dihydrochloride) to show a blue color. We assembled these spheroids into desirable patterns using our light-directed method. The cell viability was tested, revealing a high cell survival rate after laser exposure (Figure S7, Supporting Information).

Most current light-directed assembly methods require a high-power laser to produce sufficient optical forces to move individual nanoscale or sub-microscale objects, which substantially limits their throughput and bioapplication. Here, we introduced GNRs to a solution to induce thermoplasmonic convection flows, thereby enabling the assembly of large building blocks with high precision. Because significant convection flow was locally generated by heating according to light stimulation, high-throughput assembly was performed (≈ 100 building blocks per second). Moreover, a low-power infrared laser was used to trigger thermoplasmonic convection flows, which ensured minimization of cellular damage and stimulation for bioapplications. Accordingly, we used this method as a promising tool for rapid biofabrications that cannot be achieved using current assembly technology and 3D bioprinting methods. For example, functional biological building blocks^[28] were prepared before assembly to form desirable implantable biomaterials such as natural tissues with stratum structures. The separation of the assembly process and the building unit construction provides substantial flexibility in the fabrication of novel hierarchical structures.

The merit of light-directed assembly is to precisely integrate large-scale building blocks (≈ 100 μm in diameter) in a high-throughput manner using a low-power infrared laser. This technology improves the limitations of current light-directed assembly methods for the advanced fabrication of bottom-up constructions. For example, monodispersed colloids could potentially be manipulated into an assembly such as photonic crystals for optical applications.^[29] In the case of biofabrication, 3D printing technology is widely used to fabricate scaffolds or microchannels that model cell behavior in

organs for tissue engineering and drug screening. However, these technologies have reached the contradiction between cell functionality/biocompatibility and construction of desirable high-level 3D structures. Although several assembly methods have been shown to be capable of constructing functional scaffolds, challenges in precise control and throughput still remain. For example, 3D neuron-network formation can be established by a functional scaffold packed with microscaled particles; however, the network structure is not easily controlled because of an uncontrollable pore size distribution and chemical coating.^[30] A silica bead assembly was fabricated to study neuron behavior on ECMs with different topographies, but high-resolution control was difficult to attain.

3. Conclusion

In this study, a light-directed method was investigated to assemble large building blocks (≈ 100 μm in diameter) with high precision and high throughput through control of laser spot size and direction. With this advantage, a large number of building blocks were patterned and were rapidly assembled into bottom-up structures after the bonding of the assembled templates. By controlling automatic motorized stages, desirable patterns were formed with programmable manner. MSC-seeded microparticles were used to construct novel functional units for 3D cell culture with high cell viability and promising 3D proliferation. Moreover, because a low-power NIR laser was used to induce the GNR thermal convection, this method is suitable for biomedical engineering, including surgical operations and in vivo applications such as the elimination of a preshaping scaffold and prevention of contamination, as well as reagent delivery and precise cell deposition. With the capability of precisely controlled high-throughput building-block assembly, a broad array of applications is expected, ranging from 3D bioprinting to regenerative medicine, tissue engineering, bottom-up manufacturing and biofabrication.

4. Experimental Section

Fabrication of Hydrogel Microparticles: (PEGDA, GelMA) Microgels were synthesized through microfluidic encapsulation. The aqueous phase of 28 mg of photoinitiator (2-hydroxy-4'-(2-hydroxythoxy)-2-methylpropiophenone, from Sigma (PI) was dissolved in 600 μL deionized (DI) water. It was then mixed with 100 μL PEGDA (570 Mn, Sigma) and 300 μL GelMA (7.5 wt%, Biobots) as a prepolymer solution. The oil phase of fluorocarbon oil HFE 7500 (3M Novec, Singapore) with 0.5% Krytox (modified) surfactant helped stabilize the droplets. The prepolymer droplets were collected and polymerized by UV exposure (500 mW, 25 mm, 120 s). Isopropyl alcohol (IPA) was used to remove the oil and the surfactant. The hydrogel particles were washed twice with DI water to remove the IPA. Finally, the hydrogel particles were resuspended in DI water.

The Printing Systems with Automatic Stages: An XYZ customized motorized stage for 3D movement was developed for

automatic manipulation of assemblies by controlling the light spot and directions. The laser was immobilized in Z-axis stage. The wavelength of NIR laser (FC-808-2W, Optoelectronics Tech. Co., Ltd.) was 808 nm (continuous-wavelength). The laser was connected to an optical fiber (QP-400-VIS-BX) with 400 μm diameter core, which was purchased from OceanOptics Company. The distance between NIR laser and the sample (hydrogel building blocks) was set-up to a distance of 6 mm to ensure laser spot size diameter ≈ 1 mm. The Motion Controller (MICOS Company) was connected to a computer through a National Instruments (NI) USB port (USB-232/4). LabVIEW program was used to control the automatic stages. The sample was positioned on an XY-axis stage with X-axis and Y-axis control by using SMC-hydra CM 2 axis Motion Controllers.

Gold Nanorods Synthesis: GNRs were synthesized by non-seed-mediated growth.^[24] Briefly, cetyltrimethylammonium bromide (CTAB, 4.17 mL, 0.2 M), 600 μL of DI water, HAuCl_4 (60 μL , 50×10^{-3} M), AgNO_3 (50 μL , 10×10^{-3} M), ascorbic acid (50 μL , 0.1 M), and 30 μL freshly prepared 0.3 M NaBH_4 solution were mixed together in a glass flask and the resulting mixture was allowed to stand overnight at room temperature. All chemicals were purchased from Sigma-Aldrich, Inc. To precipitate GNRs, the GNR solution was centrifuged at 10 000 rpm for 30 min and then resuspended in water for further use. The GNR size was determined by TEM. The concentration and absorbance wavelength of GNRs were determined from their UV-vis spectrum (UV-2450 UV-vis spectrophotometer, Shimadzu).

Functionalization with Bovine Serum Albumin: To reduce the toxicity to cells, CTAB was replaced with BSA. To remove CTAB, the GNR solution was twice centrifuged at 12 000 rpm for 30 min. The GNRs were resuspended in a BSA solution (10 mg mL^{-1}). BSA (fraction $\geq 96\%$ lyophilized powder, for cell culture) was purchased from Sigma-Aldrich, Inc. The GNR-BSA was incubated overnight at 37 $^\circ\text{C}$, together with shaking. After incubation, the GNR-BSA was centrifuged at 10 000 rpm for 30 min to remove unbound BSA. The GNR-BSA was then resuspended in either PBS or a cell culture medium for use.

Heating Characterization: The temperature change in miliscale (around laser spot size used) was experimentally measured. In this study, the laser spot size used was around 1–2 mm in diameter to assemble microscaled hydrogel particles. To explain the phenomena reported in miliscale for high throughput assembly, miliscale temperature change to cause microconvection flow was provided in Figure 2f,g, while the on focus temperature with nanoscale was estimated by the simulation results (Figure 2d; Figure S2, Supporting Information). The nanoscale phenomena simulated were helpful to understand the mechanism and to extend the applications of proposed technology. To characterize heating phenomena, GNR suspensions (400 μL) of different concentrations (0×10^{-6} , 0.32×10^{-6} , 0.5×10^{-6} , 1.4×10^{-6} , and 2×10^{-6} M) were placed on glass as droplets. A thermocouple attached to a digital thermometer with a precision of 0.1 $^\circ\text{C}$ (Fluke 51-II) was immersed in each droplet. The GNR solution was then irradiated with an 808 nm continuous-wavelength laser (FC-808-2W, Optoelectronics Tech. Co., Ltd.) at an intensity of 2 W cm^{-2} , and the temperature was recorded for different periods of time and different laser intensities.

Chamber Size: The chamber size should be large enough, compared with the size of microconvection flow generated. In the

experiments, the height of chamber used was longer than 500 μm to ensure stable/predictable microconvection flow generated. Moreover, sufficient chamber space was prepared for microparticle movement. It was found that, if the height was less than 500 μm , the medium evaporation was too fast (within ≈ 2 min) to accomplish the wanted patterns in ≈ 10 cm scale. However, if the height of the chamber was longer than 5 mm, the heat generated by gold nanorods was not sufficient, due to limited light penetration in deep chamber area. Based on these evidences, the height of the chamber was optimized to be ≈ 2 –3 mm. The distance from laser to top of medium was ≈ 5 –6 mm.

Chemical Crosslinking of the Assembled Patterns: Hydrogel microparticles (40 μm) were assembled in fibrinogen (12.5 mg mL^{-1} , Sigma) and crosslinked by adding 10 μL thrombin (6 IU mL^{-1} , Sigma). The patterns were stabilized after 7 min by the addition of thrombin. As the concentration of thrombin was varied, the patterns crosslinked in different times.

Cell Cultures: Bone marrow was extracted from the iliac crest of Yorkshire pigs from the Tissue Sharing Program of the Institutional Animal Care and Use Committee, National University of Singapore. The MSCs were cultured in an expansion medium including of Dulbecco's modified Eagle medium (DMEM low glucose, GlutaMax supplement, Thermo Fisher Scientific) with 10% fetal bovine serum (FBS) (HyClone) and 1% penicillin/streptomycin solution (Invitrogen) in a 37 $^\circ\text{C}$, 5% CO_2 incubator. The medium was changed every 2–3 d. When cell proliferation reached 90% confluence, the cells were harvested using trypsin. These cells were considered passage 0 (p0) pBMSC cells. The p0 cells were stored in cryogenic vials in liquid nitrogen for further expansion. The cells (p1 or p2) were used for experiments in this research.

Cell-Seeded Microparticles: Hydrogel particles (PEGDA and GelMA) were sterilized in an autoclave and washed twice in PBS. The beads were seeded MSCs (p1) of ≈ 0.5 million cells per glass bottle. We used a nonadhesive surface (glass bottle) to increase cell adhesion on the beads. The cell medium was replaced every 3–4 d by gentle pipette mixing to prevent cell-seeded bead aggregation. The cells and beads were cultured in an incubator for approximately two to three weeks for assembly. The MSC-seeded microparticles were assembled into patterns and cultured in the incubator at 37 $^\circ\text{C}$ for approximately two weeks for stabilization.

Cell Viability and Proliferation Assays: A cell viability test was performed with a LIVE/DEAD (ibidi kit) staining solution by mixing 5 mL cell culture medium (w/o FBS), 8 μL FDA (5 mg mL^{-1}), and 50 μL propidium iodide (PI; 2 mg mL^{-1}). The cell-seeded microparticles and GNR-BSA (0.5×10^{-6} M) in cell culture medium solutions were irradiated for assembly using different laser intensities for various times. The cell culture medium with the GNR-BSA was then replaced with the staining solution for a 4–5 min incubation. The staining solution was removed, and PBS was added for imaging under the microscope (Olympus IX71). The live cells took up FDA and converted it to a green color, whereas the red color for the PI illustrated dead cells. The cell proliferation tests were performed with Alamar Blue (Life Technologies). MSCs (p0 or p1) were harvested in a cell culture medium with a final concentration of ≈ 10 million cells per mL^{-1} . The cell and GNR-BSA (0.5×10^{-6} M) solutions were irradiated with different laser intensities for 10 or 30 s. The irradiated cells were seeded into a 96-well plate, with ≈ 10 000 cells per well, in the incubator. The cells were measured on different days. The cells were incubated with 40 μL Alamar Blue

(Life Technologies) at 37 °C for 4 h. The staining solution was then diluted with 200 μL PBS. The resulting fluorescence was read with a microplate reader (Infinite M200 pro).

Microtissue (Spheroid) Fabrication: The cells were seeded into agarose gel microwells, which were fabricated from a casting mold (MicroTissues 3D Petri Dish Z794094 from Sigma). MSCs (200 μL of 32 000 cells) were seeded into an agarose gel mold, which was placed in a 12-well plate. After 24 h in the incubator, the cells self-organized into spheroids. The microtissues (spheroids) were collected by aspirating with a pipette for assembly. The microspheroids and GNR-BSA (0.5×10^{-6} M) in the cell culture medium solutions were irradiated for assembly. The cell viability of the spheroids was performed with a LIVE/DEAD (ibidi kit) staining solution by mixing 5 mL cell culture medium (w/o FBS), 8 μL FDA (5 mg mL^{-1}), and 50 μL PI (2 mg mL^{-1}).

Supporting Information

Supporting Information is available from the Wiley Online Library or from the author.

Acknowledgements

The authors gratefully acknowledge the funding provided by the NMRC Industry Alignment Fund Category 1 (R-397-000-230-511), NRF BDTA (R-397-000-221-592), MOE Tier-1 (R-397-000-213-112; R-397-000-248-112), A-Star PSF (R-279-000-448-305), and the facilities provided by Singapore Institute for Neurotechnology (SINAPSE). N.-D.D. and C.-H.C. designed the research. N.-D.D. performed the experiments, data analysis and written the manuscript. L.R. contributed to editing the manuscript. M.T.A.C. and J.C.-H.G. contributed to supporting the cell experiments. W.N.L. contributed to the computational simulation. W.-C.S. contributed to data analysis. C.-H.C. supervised the research and revised the manuscript. All authors discussed the results and commented on the manuscript.

- [1] C. A. DeForest, B. D. Polizzotti, K. S. Anseth, *Nat. Mater.* **2009**, *8*, 659.
- [2] G. Kumar, C. K. Tison, K. Chatterjee, P. S. Pine, J. H. McDaniel, M. L. Salit, M. F. Young, C. G. Simon Jr., *Biomaterials* **2011**, *32*, 9188.
- [3] H. O. Jacobs, A. R. Tao, A. Schwartz, D. H. Gracias, G. M. Whitesides, *Science* **2002**, *296*, 323.
- [4] G. von Freymann, V. Kitaev, B. V. Lotsch, G. A. Ozin, *Chem. Soc. Rev.* **2013**, *42*, 2528.
- [5] S. Guven, P. Chen, F. Inci, S. Tasoglu, B. Erkmen, U. Demirci, *Trends Biotechnol.* **2015**, *33*, 269.
- [6] F. Xu, T. D. Finley, M. Turkyaydin, Y. Sung, U. A. Gurkan, A. S. Yavuz, R. O. Guldiken, U. Demirci, *Biomaterials* **2011**, *32*, 7847.
- [7] F. Xu, C.-A. M. Wu, V. Rengarajan, T. D. Finley, H. O. Keles, Y. Sung, B. Li, U. A. Gurkan, U. Demirci, *Adv. Mater.* **2011**, *23*, 4254.
- [8] P. Chen, Z. Luo, S. Guven, S. Tasoglu, A. V. Ganesan, A. Weng, U. Demirci, *Adv. Mater.* **2014**, *26*, 5936.
- [9] D. R. Griffin, W. M. Weaver, P. O. Scumpia, D. Di Carlo, T. Segura, *Nat. Mater.* **2015**, *14*, 737.
- [10] S. E. Chung, W. Park, S. Shin, S. A. Lee, S. Kwon, *Nat. Mater.* **2008**, *7*, 581.
- [11] Y. Du, E. Lo, S. Ali, A. Khademhosseini, *Proc. Natl. Acad. Sci. USA* **2008**, *105*, 9522.
- [12] H. Qi, M. Ghodousi, Y. Du, C. Grun, H. Bae, P. Yin, A. Khademhosseini, *Nat. Commun.* **2013**, *4*, 2275.
- [13] S. Tasoglu, C. H. Yu, H. I. Gungordu, S. Guven, T. Vural, U. Demirci, *Nat. Commun.* **2014**, *5*, 4702.
- [14] S. Tasoglu, E. Diller, S. Guven, M. Sitti, U. Demirci, *Nat. Commun.* **2014**, *5*, 3124.
- [15] M. Y. Chiang, Y. W. Hsu, H. Y. Hsieh, S. Y. Chen, S. K. Fan, *Sci. Adv.* **2016**, *2*, e1600964.
- [16] a) S. V. Murphy, A. Atala, *Nat. Biotechnol.* **2014**, *32*, 773; b) H. W. Kang, S. J. Lee, I. K. Ko, C. Kengla, J. J. Yoo, A. Atala, *Nat. Biotechnol.* **2016**, *34*, 312.
- [17] T. J. Hinton, Q. Jallerat, R. N. Palchesko, J. H. Park, M. S. Grodzicki, H.-J. Shue, M. H. Ramadan, A. R. Hudson, A. W. Feinberg, *Sci. Adv.* **2015**, *1*, e1500758.
- [18] D. G. Grier, *Nature* **2003**, *424*, 810.
- [19] P. Y. Chiou, A. T. Ohta, M. C. Wu, *Nature* **2005**, *436*, 370.
- [20] H. Xin, Y. Li, B. Li, *Adv. Funct. Mater.* **2015**, *25*, 2816.
- [21] B. J. Roxworthy, A. M. Bhuiya, S. P. Vanka, K. C. Toussaint Jr., *Nat. Commun.* **2014**, *5*, 3173.
- [22] J. C. Ndukaife, A. Mishra, U. Guler, A. G. Nnanna, S. T. Wereley, A. Boltasseva, *ACS Nano* **2014**, *8*, 9035.
- [23] P. J. Dobson, *Contemp. Phys.* **2014**, *55*, 352.
- [24] T. K. Sau, C. J. Murphy, *Langmuir* **2004**, *20*, 6414.
- [25] P. Haro-González, P. R. Sevilla, F. Sanz-Rodríguez, E. M. Rodríguez, N. Bogdan, J. A. Capobianco, K. Dholakia, D. Jaque, *Opt. Express* **2014**, *22*, 19735.
- [26] W. Hu, K. S. Ishii, Q. Fan, A. T. Ohta, *Lab Chip* **2012**, *12*, 3821.
- [27] U. A. Gurkan, S. Tasoglu, D. Kavaz, M. C. Demirel, U. Demirci, *Adv. Healthcare Mater.* **2012**, *1*, 149.
- [28] A. Leferink, D. Schipper, E. Arts, E. Vrij, N. Rivron, M. Karperien, K. Mittmann, C. van Blitterswijk, L. Moroni, R. Truckenmuller, *Adv. Mater.* **2014**, *26*, 2592.
- [29] Q. M. Zhang, W. Xu, M. J. Serpe, *Angew. Chem., Int. Ed.* **2014**, *53*, 4827.
- [30] K. Kang, S. Y. Yoon, S. E. Choi, M. H. Kim, M. Park, Y. Nam, J. S. Lee, I. S. Choi, *Angew. Chem., Int. Ed.* **2014**, *53*, 6075.

Received: March 1, 2017
Published online: May 8, 2017